Aeroacoustic characterisation of single and dual tooth-shaped obstacle replicas in relation to the study of unvoiced fricative speech production

Y. Fujiso and A. Van Hirtum

Gipsa-lab, UMR CNRS 5126, Grenoble Universities, 38000 Grenoble, France
yo.fujiso@gipsa-lab.grenoble-inp.fr

Unvoiced fricative speech production involves the noise produced by a complex fluid-structure interaction between a moderate bulk Reynolds number ($100 < Re < 10000$) turbulent jet issued from a constriction somewhere in the vocal tract with a downstream obstacle (i.e. articulators such as lips, tongue or teeth). To contribute to the physical study of human unvoiced fricative speech production, two types of simplified in-vitro teeth-shaped (single and dual) obstacle replicas are experimentally investigated. Acoustic measurements of the noise emitted by an airflow passing through each of the two replicas are performed at several moderate bulk Reynolds numbers relevant to fricative production in a quasi-anechoic chamber. In order to characterise and quantify the influence of articulators position and shape on the produced sound, various geometric parameters of the replicas are tested. Furthermore, the effect of initial and boundary conditions are studied as well by varying them.

1 Introduction

Unvoiced speech production means that the vocal folds do not vibrate during the production of such speech sounds. Compared to voiced speech production, unvoiced sounds have been far less studied. Unvoiced fricative consonants, such as [f] and [s], are produced by a turbulent airflow interacting with various articulators of the vocal tract (such as lips, teeth or tongue) and passing through constrictions (i.e. sudden narrowings in the vocal tract due to the presence of the above mentioned obstacles). Such airflows are characterised by moderate Reynolds ($10^2 < Re < 10^4$) and low Mach numbers ($M < 0.2$) [6]. The main underlying acoustic mechanisms of fricative sound production are outlined by Shadle [4]. However, the way a turbulent airflow produces unvoiced fricative sounds as well as where this sound production occurs are still far from being completely understood.

Although several aeroacoustic models of the sibilant fricative production using simplified or realistic *in-vitro* replicas of the vocal tract and/or teeth were proposed (e.g. [2]), the influence of geometric parameters on the properties of the sound generated remains an open question. Indeed, small variations of the position of the articulators (tongue and teeth) significantly change the spectral properties of the sound generated according to *in-vivo* [3] and *in-vitro* [5] studies. Compared to realistic ones, simplified *in-vitro* replicas have the advantage of reducing the complexity of the study by focusing on a limited number of phenomena and parameters. Moreover, geometric parameters in simplified replicas can be quite easily controlled and an overall higher experimental repeatability can be achieved.

In this article, two types of simplified two-dimensional *in-vitro* teeth-shaped obstacle replicas are presented: a single and a dual-teeth geometry. The single replica has already been experimentally and numerically studied by Grandchamp *et al* [1], but only at a bulk Reynolds number of 4000, and has not been acoustically characterised. The dual-teeth replica has not been studied before. With two teeth-shaped obstacles instead of one, this replica is closer to the *in-vivo* morphology. For both replicas, the aim is to study the influence of various geometric parameters on the noise produced at the constriction (i.e. the space created under or between the teeth-shaped obstacle(s)) when an airflow passes through the replica at different volume flow rates relevant to speech production. Spectral characteristics of the measured noises at 4 different Reynolds numbers relevant to speech production are compared and discussed.

2 Description of the two replicas

2.1 Single teeth-shaped obstacle replica

The geometry of the two-dimensional single teeth-shaped obstacle replica (Fig. 1) is based upon two main morphological characteristics: (1) upper incisor dimensions in the flow direction and (2) upper teeth position with respect to the palatal plane. The obstacle has the shape of a trapezoid defined by its base l_{pal} = 6.6mm, tip length l_t = 1.25mm and height h_t = 17.5mm. In the standard configuration, the leading and trailing angles of the obstacle with the upper plane of the rectangular channel are $\theta_1 = 107°$ and $\theta_2 = 90°$, which corresponds to the orders of magnitudes observed in *in-vivo* subjects [1]. The obstacle can be inverted as well and in this case $\theta_1 = 90°$ while $\theta_2 = 107°$. The degree of aperture, defined by the ratio between the unconstricted and constricted heights $\frac{h}{h_0}$, can be accurately fixed by a screw.

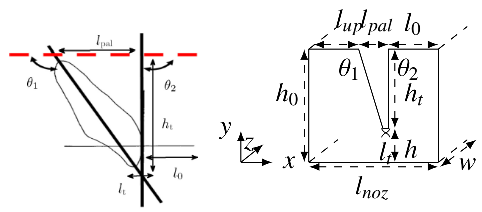

(a) (b)

Figure 1: (a) Incisor model [7] (b) Single teeth-shaped obstacle replica [1]

2.2 Dual teeth-shaped obstacle replica

The two-dimensional dual teeth-shaped obstacle replica is composed of two obstacles which have exactly the same shape and dimensions as the teeth of the single obstacle replica (Fig. 2), for which corresponding heights h_t and h'_t can be both precisely adjusted by screws. The two obstacles can be positioned symmetrically (i.e. $\theta_1 = 107°$, $\theta_2 = 90°$, $\theta'_1 = 107°$, $\theta'_2 = 90°$) or asymmetrically (i.e. $\theta_1 = 107°$, $\theta_2 = 90°$, $\theta'_1 = 90°$, $\theta'_2 = 107°$). The height difference between both obstacles is arbitrarily defined as the constricted height h for this replica. h can be either positive (i.e. open teeth as in the current paper) or negative (i.e. overbite). It is arbitrarily chosen to vary only the height of the lower teeth while fixing the height of the upper one.

3 Aeroacoustic measurement set-up

The aeroacoustic measurement set-up used for both replicas is schematically depicted in Fig. 3. The apparatus is

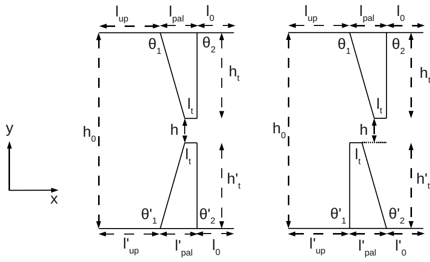

Figure 2: Dual teeth-shaped obstacle replica: symmetric teeth (left) and asymmetric teeth (right) configurations. Positive *x*-axis direction is the mainstream direction.

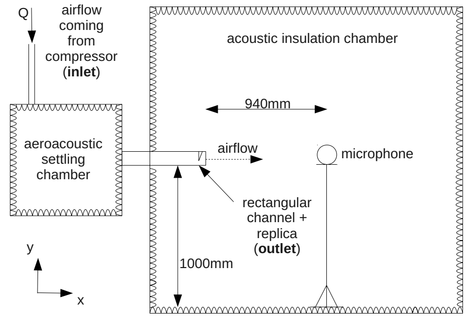

Figure 3: Measurement set-up used for both replicas

mainly composed of the following items:

- Air compressor (Atlas Copco GA7, located outside the experiment room) coupled to a pressure regulator (Norgren type 11-818-987), which provides the inlet airflow. The volume flowrate Q of the inlet airflow is adjusted by a valve and measured by a volume flowmeter (TSI 4000 Series).

- Aeroacoustic settling chamber made of plexiglas, with internal walls covered by acoustic foam (SE50-AL-ML, Elastomeres Solutions), to limit the upstream noise created in the inlet flow and to avoid any disturbing acoustic resonance.

- Acoustic insulation chamber (dimensions $2.07\times2.10\times2.14$m), to isolate from noise inherent to the measurement set-up, to ensure a low background noise and to avoid any sound reflection (quasi-anechoic conditions) during measurements, as described in [8]. The kinematic viscosity of air ν inside the insulation chamber was nearly constant during all measurements ($\nu \approx 1.5 \cdot 10^{-5}\mathrm{m}^2/\mathrm{s}$).

- Uniform unconstricted rectangular channel (length L of 310 or 620mm, internal width $w = 105$mm, internal height $h_0 = 25$mm), made of plexiglas, at the end of which the replica to be tested is mounted. The main purpose of this channel is to avoid a *vena-contracta* effect and to simulate the vocal tract presence upstream of the oral cavity in a very simplified manner. In order to reduce the turbulence inside a given channel, a honeycomb with hexagonal cavities of diameter 9mm and length 80mm can be inserted at the upstream end of the channel.

- Pressure-field microphone B&K type 4192 (+ preamplifier B&K type 2669) installed at a position not too close to any wall of the insulation chamber and to the replica outlet (94cm), for recording the pressure variations inside the chamber. The microphone is located at the same height as the replica but with an angle of about 37 ° with respect to the main flow direction x in the horizontal plane, in order to avoid any disturbance from the flow on the microphone, which is not protected by a wind-shield. It is supplied and amplified (+30dB) by a B&K amplifier type 5935.

3.1 Flow characterisation of inlet conditions

To characterise the airflow for each volume flowrate, a bulk Reynolds number Re_b based upon the adjustable constricted height h and width w of the rectangular channel is defined as

$$Re_b = \frac{U_b h}{\nu} = \frac{Q}{w\nu}, \tag{1}$$

where $U_b = \frac{Q}{wh}$ is the bulk velocity at the constricted section with rectangular area wh. Since the width w remains constant for all the tested configurations, the bulk Reynolds number depends only on the volume flow rate Q and not on the degree of aperture $\frac{h}{h_0}$. In the current study, the following inlet volume flowrates are used: 60, 100, 160, 200L/min, respectively corresponding to the bulk Reynolds numbers 606, 1010, 1616, 2020, relevant to speech production ($10^2 < Re_b < 10^4$).

Four different types of inlet conditions are tested: (1) no rectangular channel inserted between the replica and the settling chamber, (2) 310mm-channel, (3) 620mm-channel, (4) honeycombed 310mm-channel. Prior to the acoustic measurements, it is useful to characterise the airflow properties at the outlet sections of these inlet conditions (with no replica) i.e. at the locations where the replica is normally mounted. Interesting airflow properties are the transverse distributions of local longitudinal mean velocities $\bar{U}(y)$ and corresponding local turbulence intensities $T_u(y) = 100 \cdot \frac{\sigma(y)}{\bar{U}(y)}$, with $\sigma(y)$ the standard deviation of $U(y)$.

Velocity profiles of the four tested inlet conditions measured at outlet sections are shown in Fig. 4 and corresponding local turbulence intensities are shown in Fig. 5. The six Reynolds numbers of these figures are different from the four ones used for the acoustic measurements because they correspond to another study focusing on flow properties of a larger number of inlet conditions, which was conducted independently. Nevertheless, these Reynolds numbers are in the same order so comparison is relevant. Theoretical profiles are added for comparison: parabolic (laminar), power law 1/7 (turbulent), top hat (turbulent) and uniform (ideal fluid) profiles. At least for higher Reynolds numbers (751, 1114, 1296), the experimental profiles seem clearly turbulent (not parabolic), and follow either a power law or a top hat behaviour. A much higher turbulence intensity is found for the 'no-channel' case (Fig. 5(a)), especially near the walls (40-50%).

4 Acoustic results and discussion

4.1 Spectral characterisation of acoustic data

For each tested configuration and each volume flowrate, the pressure time signal was recorded during five seconds at a sampling rate of 44.1kHz. Spectral characterisation of the

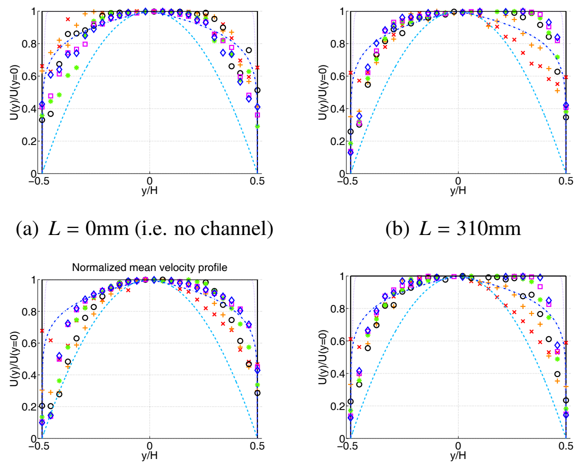

(a) L = 0mm (i.e. no channel) (b) L = 310mm

(c) L = 310mm + honeycomb (d) L = 620mm

Figure 4: Normalized mean transverse velocity profiles measured at the outlet of tested inlet conditions (without attached replica) for 6 bulk Reynolds numbers: 114 (×), 296 (+), 478 (∘), 751 (∗), 1114 (□), 1296 (⋄). Theoretical profiles are added for comparison: parabolic (dashed), power law 1/7 (dash-dot), top hat (dotted), uniform (solid).

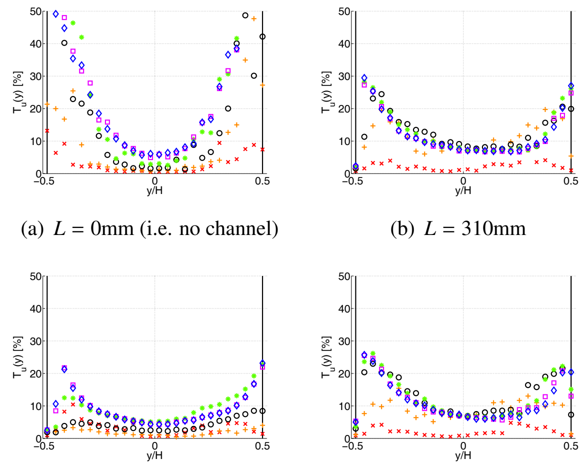

(a) L = 0mm (i.e. no channel) (b) L = 310mm

(c) L = 310mm + honeycomb (d) L = 620mm

Figure 5: Local transverse turbulence intensities measured at the outlet of tested inlet conditions (without attached replica) for 6 bulk Reynolds numbers: 114 (×), 296 (+), 478 (∘), 751 (∗), 1114 (□), 1296 (⋄).

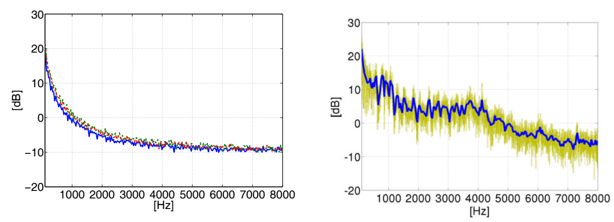

(a) (b)

Figure 6: (a) Background noise (4 repeated measurements) (b) Raw (solid) and corresponding filtered signal (dotted)

measured acoustic data is carried out by estimating power spectral densities (PSD) of the pressure time signals recorded by the microphone. Since all these signals are random and unsteady, mainly due to turbulent fluctuations, Welch's periodogram method is used for PSD estimation in order to improve the signal-to-noise ratio (5 one second segments and 10% overlap). Signals are high-pass filtered by a Butterworth filter of 5th order and a cut-off frequency of 50Hz (Fig. 6(b)). Frequencies of interest are between 100 and 8000Hz, relevant to speech production. All the presented spectra figures show the sound pressure levels (SPL) in the frequency domain, expressed in dB/Hz and defined as

$$L_p(f) = 10 \cdot \log_{10}\left(\frac{|P(f)|}{p_{ref}^2}\right), \tag{2}$$

where $p_{ref} = 2 \cdot 10^{-5}$Pa and $P(f)$ is the PSD estimation of the measured pressure samples. In the presented figures, the symbol dB stands for dB/Hz. The background noise inside the insulation chamber was measured before each measurement. The repeatability of the background noise is verified as illustrated in Fig. 6(a).

4.2 Results for the single obstacle replica

In addition to the bulk Reynolds number, the other tested parameters for the single obstacle replica are listed in Table 1. Among the four types of inlet conditions, in order to reduce the number of distinct combinations of parameters to test, the empty 310mm-channel (i.e. without honeycomb) is arbitrarily chosen as a standard configuration when varying the other parameters since its length is closer to that of a real vocal tract (169mm in average for males [6]).

First, the influence of the degree of aperture $\frac{h}{h_0}$ is studied for the case of an empty 310mm-channel and a leading angle $\theta_1 = 107°$ (Fig. 7). For 30% aperture, nearly no noise is produced for all Reynolds numbers. However, as expected from [4], significant noise is produced for smaller apertures and higher Reynolds numbers, i.e. for higher pressure drops across the constriction. For 2.4% aperture and $Re_b = 2020$, the spectrum has a broadband shape, similar to that of fricative noise [4], with an increased presence of high frequency peaks. Since much more noise is generated for this degree of aperture, it is chosen to maintain the degree of aperture at 2.4% when varying the subsequent parameters.

Next, the influence of the leading angle θ_1 is studied for the two values of 107° (standard) and 90° (inverted position) with L = 310mm and $\frac{h}{h_0}$ = 2.4%. Corresponding results are shown in Fig. 8. Although the overall noise levels are slightly higher for $\theta_1 = 107°$, the two angle configurations do not exhibit significant differences. Observed peaks are at the same frequencies for both configurations.

Then, the length of the rectangular channel is varied (L = 0, 310, 620mm) for an aperture of 2.4% and a leading angle $\theta_1 = 90°$, without any honeycomb inserted. Varying L for $\theta_1 = 107°$ has not been carried out yet. From Fig. 9, it appears that the longer the channel, the lower the generated noise. This is probably because the channel tends to reduce the turbulence upstream of the replica. Moreover, when no channel is inserted, the replica is directly connected to the aeroacoustic settling chamber by an abrupt contraction with sharp edges, where a *vena-contracta* effect may occur and where a substantial number of eddies may be generated, becoming an additional source of noise. This is consistent with the high turbulence intensities visible on Fig. 5(a).

Table 1: Tested parameters for the single obstacle replica (HC = honeycomb)

Re_b [-]	606 - 1010 - 1616 - 2020
$\frac{h}{h_0}$ [%]	2.4 - 10 - 30
L [mm]	0 - 310 - 620 - 310+HC
θ_1 [°]	90 - 107

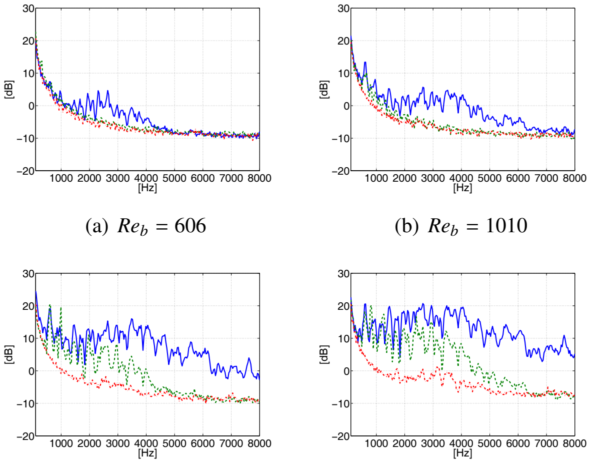

(a) Re_b = 606 (b) Re_b = 1010

(c) Re_b = 1616 (d) Re_b = 2020

Figure 7: Influence of the degree of aperture $\frac{h}{h_0}$ for the single obstacle replica (L = 310mm and θ_1 = 107°): 2.4% (solid) - 10% (dashed) - 30% (dash-dot)

Finally, the acoustic effects of inserting the honeycomb described in Section 3 inside the 310mm-channel with the single obstacle replica mounted are illustrated in Fig. 10. As expected, less noise is radiated when the channel is honeycombed, especially for lower Reynolds numbers. Indeed, the honeycomb reduces the turbulence effects by homogenising the streamlines of the airflow and reducing the eddies.

4.3 Results for the dual obstacle replica

For the dual obstacle replica, the symmetrically and asymmetrically positioned teeth configurations (Fig. 2) are studied. Only the unhoneycombed 310mm-channel is used as inlet condition for the two configurations. The same degrees of aperture $\frac{h}{H_0}$ as for the single obstacle replica are used (2.4, 10 and 30%). Results for the symmetric case are displayed in Fig. 11 while Fig. 12 shows results for the asymmetric case.

From these figures, it can be concluded that for the dual obstacle replica, the degree of aperture does not exhibit a significant influence on the produced noise, at least for the tested values, whether the teeth are symmetric or not and even for higher Reynolds numbers. This shows that the presence of a horizontal surface in the vicinity of the constriction, as the case for the single obstacle replica, leads to a more efficient noise radiation. Indeed, for the dual obstacle replica, the upper and lower walls of the rectangular channel upstream of the two teeth are located relatively far from the constriction formed by the teeth. This phenomenon could be compared to the *in-vivo* sibilant production, for which it is easier to produce a [*s*] by moving the tongue closer to the incisors than keeping the tongue far away from them.

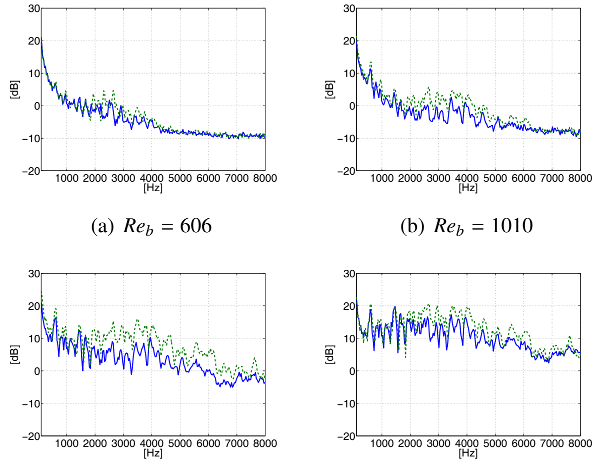

(a) Re_b = 606 (b) Re_b = 1010

(c) Re_b = 1616 (d) Re_b = 2020

Figure 8: Influence of the leading angle θ_1 for the single obstacle replica (L = 310mm and $\frac{h}{h_0}$ = 2.4%): 90° (solid) - 107° (dashed)

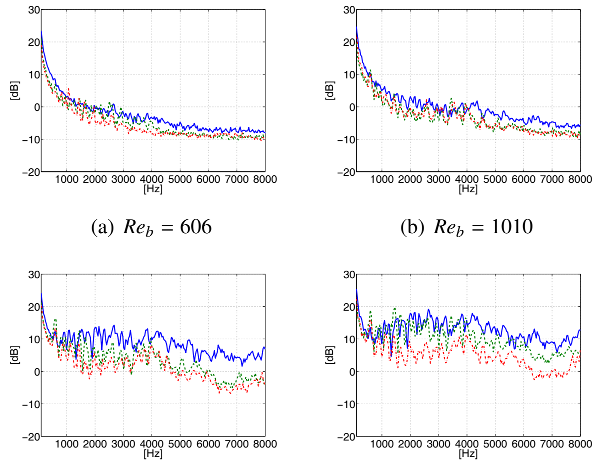

(a) Re_b = 606 (b) Re_b = 1010

(c) Re_b = 1616 (d) Re_b = 2020

Figure 9: Influence of the rectangular channel length L for the single obstacle replica ($\frac{h}{h_0}$ = 2.4% and θ_1 = 90°): 0mm (solid) - 310mm (dashed) - 620mm (dash-dot)

5 Conclusion

The current paper presents an experimental aeroacoustic study of a single and a dual teeth-shaped obstacle replica, which are simplified *in-vitro* models of a human *in-vivo* oral cavity coupled with incisors. Various bulk Reynolds numbers relevant to speech production and various geometric parameters are tested for both replicas. For the single obstacle replica, the degree of aperture, as expected from [4], is a key parameter for fricative noise production. Indeed, a smaller degree of aperture, i.e. a higher pressure drop across the constriction, leads to higher noise radiation.

Although the dual obstacle replica is morphologically closer to the *in-vivo* reality, with the presence of two teeth instead of one, noises generated by a turbulent airflow passing through the single obstacle replica seem acoustically closer

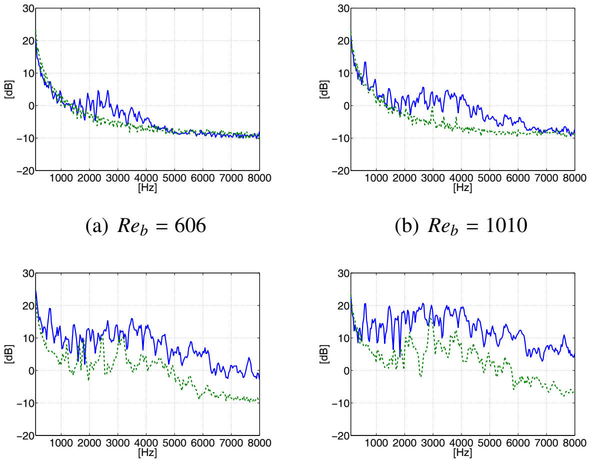

(a) Re_b = 606 (b) Re_b = 1010

(c) Re_b = 1616 (d) Re_b = 2020

Figure 10: Effect of inserting a honeycomb into a 310mm-channel with attached single obstacle replica (θ_1 = 107 °): empty channel (solid) - honeycombed (dashed)

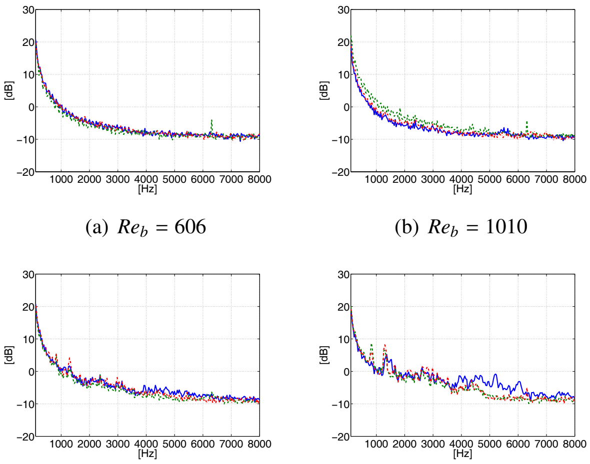

(a) Re_b = 606 (b) Re_b = 1010

(c) Re_b = 1616 (d) Re_b = 2020

Figure 11: Influence of the degree of aperture $\frac{h}{h_0}$ for the dual obstacle replica with symmetric teeth configuration: 2.4% (solid) - 10% (dashed) - 30% (dash-dot)

to real unvoiced fricative sibilant speech sounds, at least under the tested conditions. This is probably because the presence of a horizontal surface in the vicinity of the constriction, which interacts with the flow, is required to achieve a more efficient fricative noise generation.

However, for a deeper characterisation of these two replicas, other values of the studied geometric parameters should be tested, as well as extending the Reynolds numbers and frequency range. The overbite configuration for the dual obstacle replica is an avenue worth investigating. Another interesting parameter which has not been explored yet is the directivity of the produced noises, as it may bring further clarifications about the location of fricative noise production in the oral cavity system. Building and testing a two-dimensional circular teeth-shaped obstacle could provide interesting results as well, for understanding the influence of the teeth row shape on the produced sound. Finally, aeroacoustic numerical models of the experimentally tested configurations could be implemented and numerical results could be compared with the experimental results.

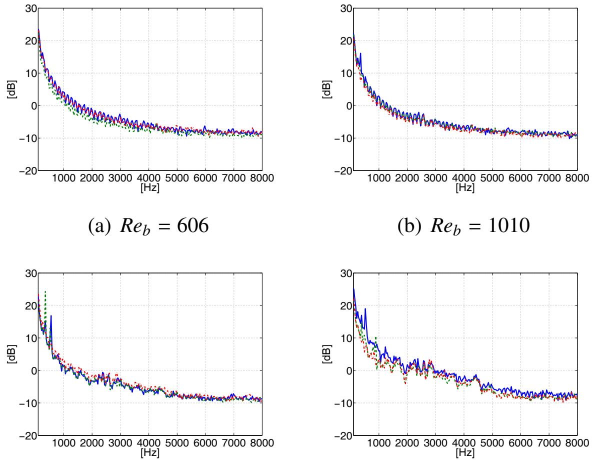

(a) Re_b = 606 (b) Re_b = 1010

(c) Re_b = 1616 (d) Re_b = 2020

Figure 12: Influence of degree of aperture $\frac{h}{h_0}$ for the dual obstacle replica with asymmetric teeth configuration: 2.4% (solid) - 10% (dashed) - 30% (dash-dot)

Acknowledgements

Financial support of Agence Nationale de Recherche (Petaflow ANR-09-BLAN-0376-01) is gratefully acknowledged.

References

[1] X. Grandchamp, A. Van Hirtum, K. Nozaki, J. Cisonni, X. Pelorson, "Visualisation of moderate Reynolds number flow through a teeth-shaped nozzle", *in Proc. 20th International Congress on Acoustics* (2010)

[2] K. Nozaki, "Numerical Simulation of Sibilant [s] Using the Real Geometry of a Human Vocal Tract", *in Proc. High Performance Computing on Vector Systems, Springer Berlin Heidelberg*, 137-148 (2010)

[3] C. Runte, M. Lawerino, D. Dirksen, F. Bollmann, A. Lamprecht-Dinnesen, E. Seifert, "The influence of maxillary central incisor position in complete dentures on /s/ sound production", *The journal of prosthetic dentistry*, **85**(5), 485-495 (2001)

[4] C.H. Shadle, "The acoustics of fricative consonants", PhD thesis, MIT, *Dept. of Electrical Engineering and Computer Science* (1985)

[5] C.H. Shadle, M. Berezina, M. Proctor, K. Iskarous, "Mechanical models of fricatives based on MRI-derived vocal tract shapes", *in Proc. 8th International Seminar on Speech Production (ISSP)* (2008)

[6] K.N. Stevens, *Acoustic phonetics*, MIT press (2000)

[7] A. Van Hirtum, X. Grandchamp, X. Pelorson, K. Nozaki, S. Shimojo, "LES and 'in-vitro' experimental validation of flow around a teeth-shaped obstacle", *Int. J. of Applied Mechanics*, **2**, 265-279 (2010)

[8] A. Van Hirtum, Y. Fujiso, "Insulation room for aeroacoustic experiments at moderate Reynolds and low Mach numbers", *Applied Acoustics*, **73**, 72-77 (2012)